SUPPLEMENTARY FIGURES

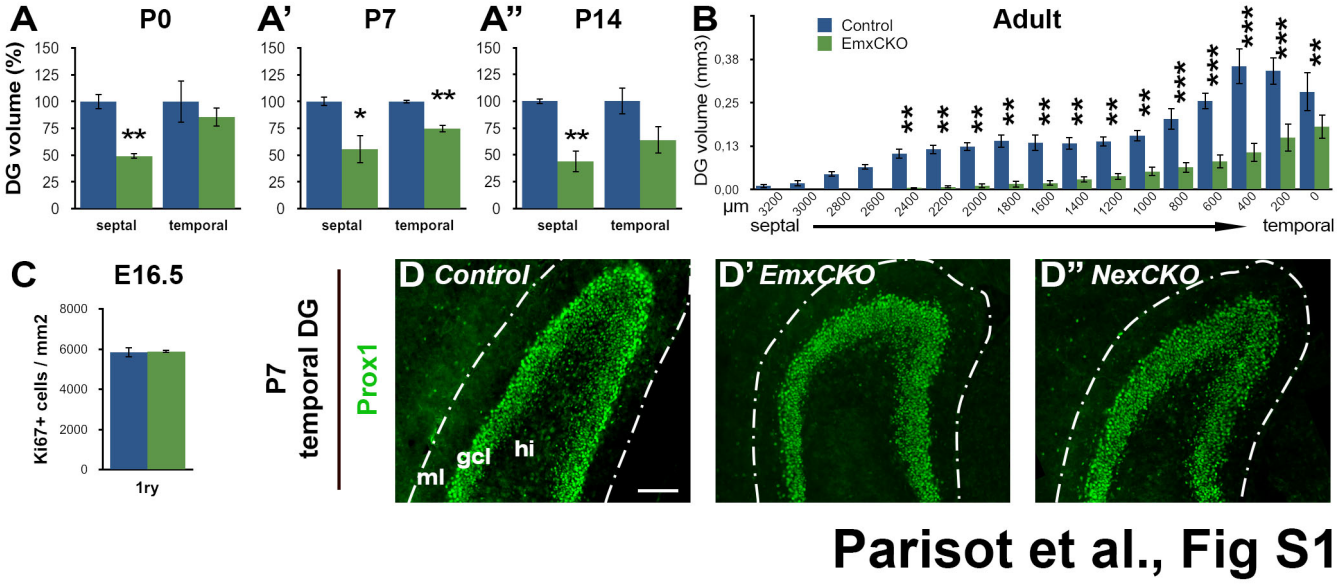

Figure S1. COUP-TFI loss in progenitors affects mainly the septal dentate gyrus (DG). **(A-A")** Quantification of septal and temporal DG volumes in control and *EmxCKO* mutants, set up to 100% of controls at P0 (A), P7 (A') and P14 (A"), shows a stronger volume decrease in the septal than temporal pole. **(B)** Septo-temporal distribution of DG volume in the adult. **(C)** No changes in the density of Ki67+ cycling cells in the temporal 1ry matrix of *EmxCKO* DG at E16.5. **(D-D")** Temporal DG lamination labelled by Prox1 in P7 *EmxCKO* and *NexCKO* DGs indicates no particular accumulation of Prox1+ cells in the hilus (as instead observed in the septal pole, see Fig. 5E'). *gcl: granule cell layer; hi: hilus; ml: molecular layer. Scale bar: 100µm. *p≤0,05; **p≤0,01; ***p≤0,001.*

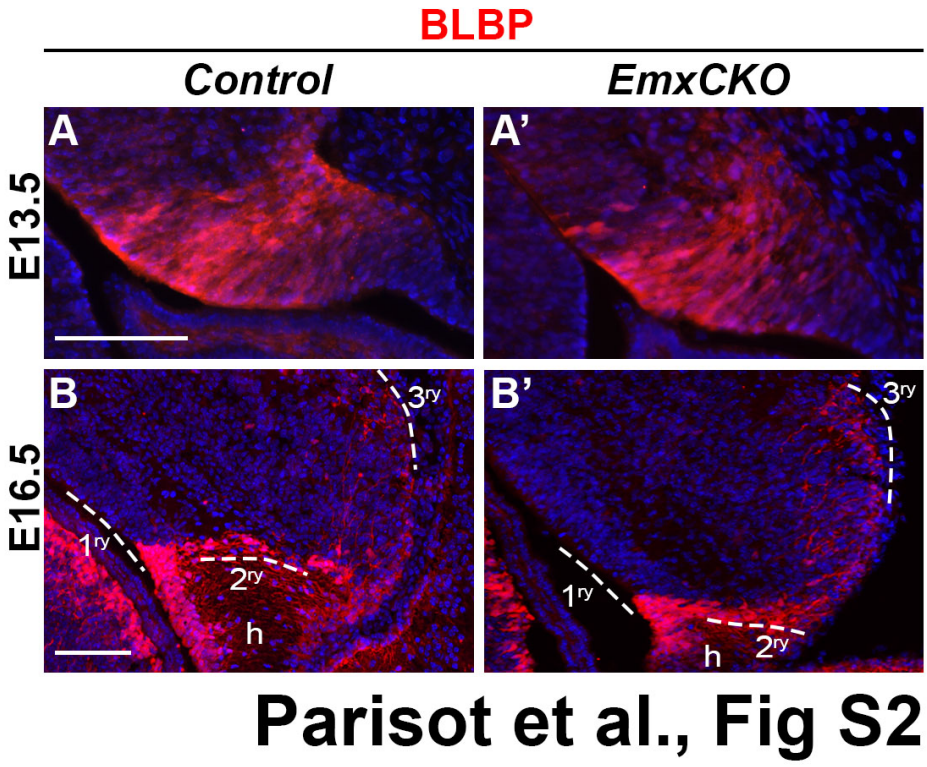

Figure S2. No obvious defects in the embryonic scaffold in the absence of COUP-TFI in progenitors. (A-A') BLBP immunostaining on the primordial hippocampus in E13.5 control and *EmxCKO* embryos. **(B-B')** BLBP immunostaining on the developing DG in E16.5 control and *EmxCKO* embryos. At both developmental stages, BLBP+ cells are mainly located around the cortical hem with few fibres extending to the 3^{ry} matrix in controls and *EmxCKO* embryos. *h: cortical hem. Scale bar: 100µm.*

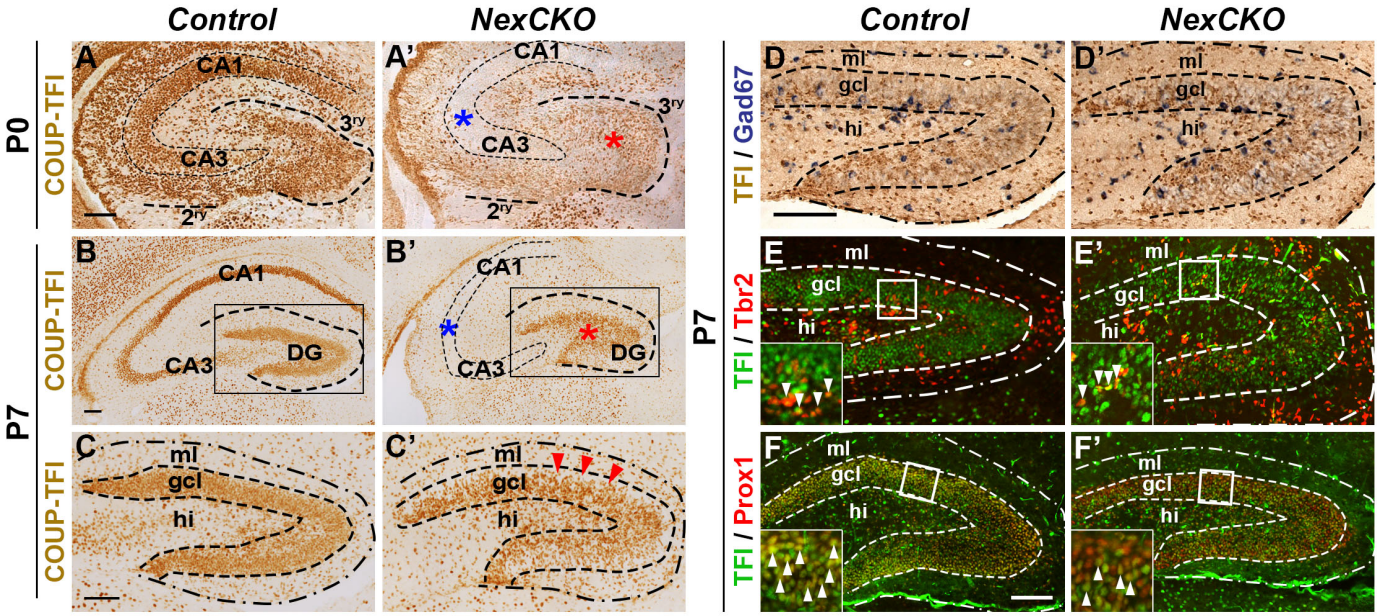

Parisot et al., Fig S3

Figure S3. COUP-TFI is depleted in late postmitotic granule cells of the *NexCKO* dentate gyrus (DG). (A-C') COUP-TFI immunostaining in control and *NexCKO* post-natal hippocampal coronal sections at P0 (A-A') and P7 (B-C'). Blue asterisks in A'-B' support the expected loss of COUP-TFI expression in postmitotic pyramidal cells of CA1-3, whereas red asterisks highlight decrease of COUP-TFI-expressing cells in the DG. (C-C') High magnification views of the boxes in B-B'. Red arrowheads in C' indicate complete loss of COUP-TFI protein in the external one-third of the GC layer (gcl), where more mature GCs are located, whereas expression is only slightly decreased in the inner two-third where progenitors and precursors are still maintained. **(D-D')** Double staining for COUP-TFI protein (IHC) and *Gad67* expression (ISH) in P7 control and mutant DGs. The number and distribution of COUP-TFI+ interneurons appear similar to control in *NexCKO* DGs. **(E-F')** Co-expression of COUP-TFI in Tbr2+ (E-E') and Prox1+ cells (F-F') in control and *NexCKO* DGs at P7. Arrowheads in insets indicate double-labelled cells and indicate that COUP-TFI is still expressed in Tbr2+ IPC, and in some Prox1+ granule precursors. *gcl: granule cell layer; hi: hilus; ml: molecular layer. Scale bars: 100µm.*

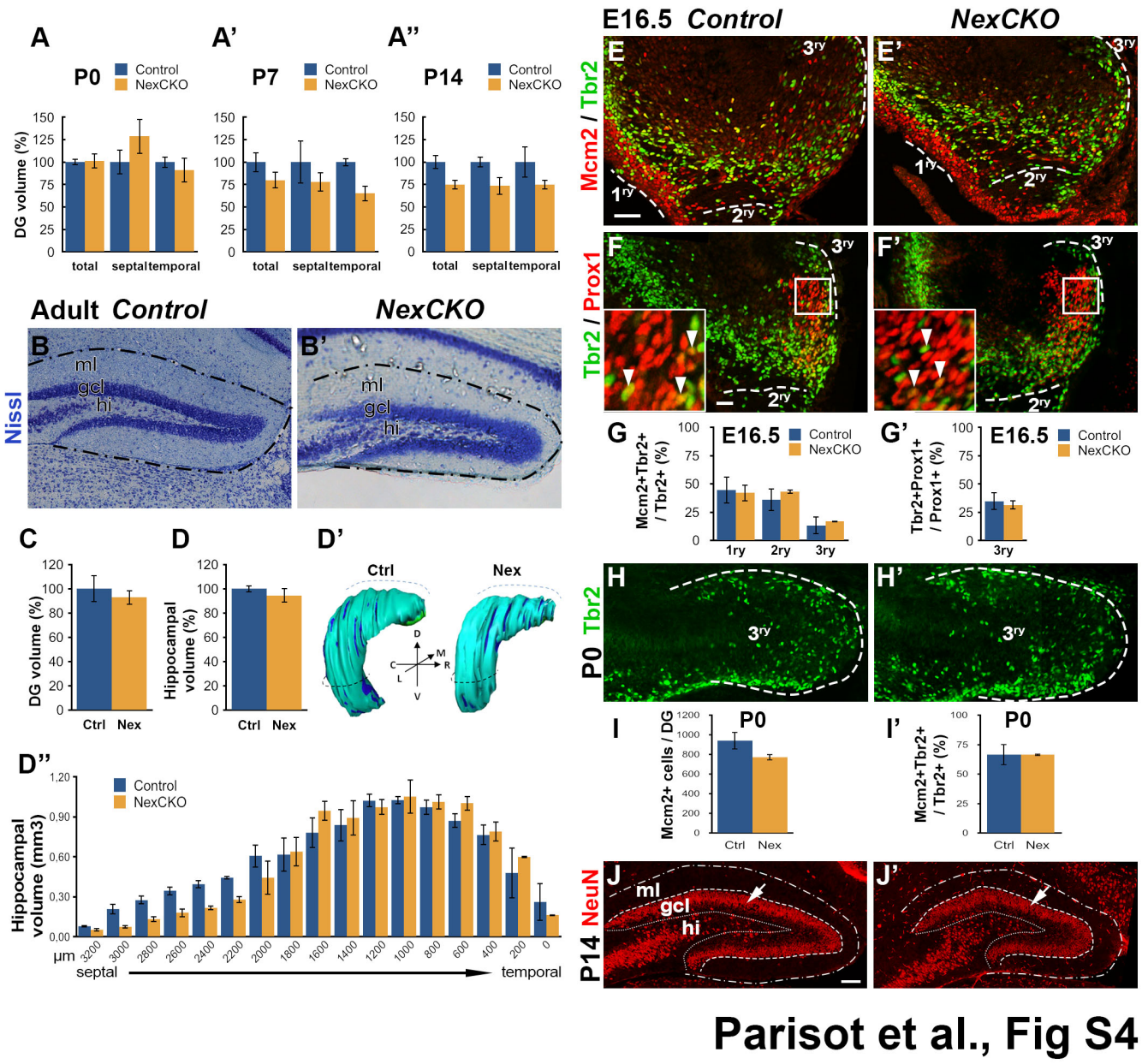

Parisot et al., Fig S4

Figure S4. Loss of COUP-TFI function in postmitotic cells does not affect growth and granule cell differentiation. (A-A") Volume of total, septal and temporal control and *NexCKO* DG at P0, P7 and P14. **(B-C)** Nissl staining of adult septal DG and total DG volume (C) show no significant differences between control and mutants. **(D-D")** Global hippocampal volume is not affected in adult *NexCKO* brains (D). D' represents a 3D reconstruction of control and *NexCKO* hippocampi and D" corresponds to the septo-temporal distribution of hippocampal volume. **(E-F')** Co-expression of Mcm2/Tbr2 and Tbr2/Prox1 in E16.5 control

and *NexCKO* DGs. The amount of Tbr2+ IPC expressing the cell cycle marker Mcm2 (G) and the amount of Prox1+ GCs expressing Tbr2 (G') are not changed between controls and mutant DGs. **(H-H')** Tbr2+ IPCs in P0 *NexCKO* DGs are found in similar number and distribution to controls. **(I-I')** Mitotic Mcm2+ cells are not affected in *NexCKO* DGs (F), nor the proliferative capacity of IPCs (F'). **(J-J')** Expression and distribution of the mature neuronal marker NeuN is found in the external two-third of the granule cell layer (gcl) in control and *NexCKO* DGs. *hi: hilus; ml: molecular layer. Scale bars: 100µm.*

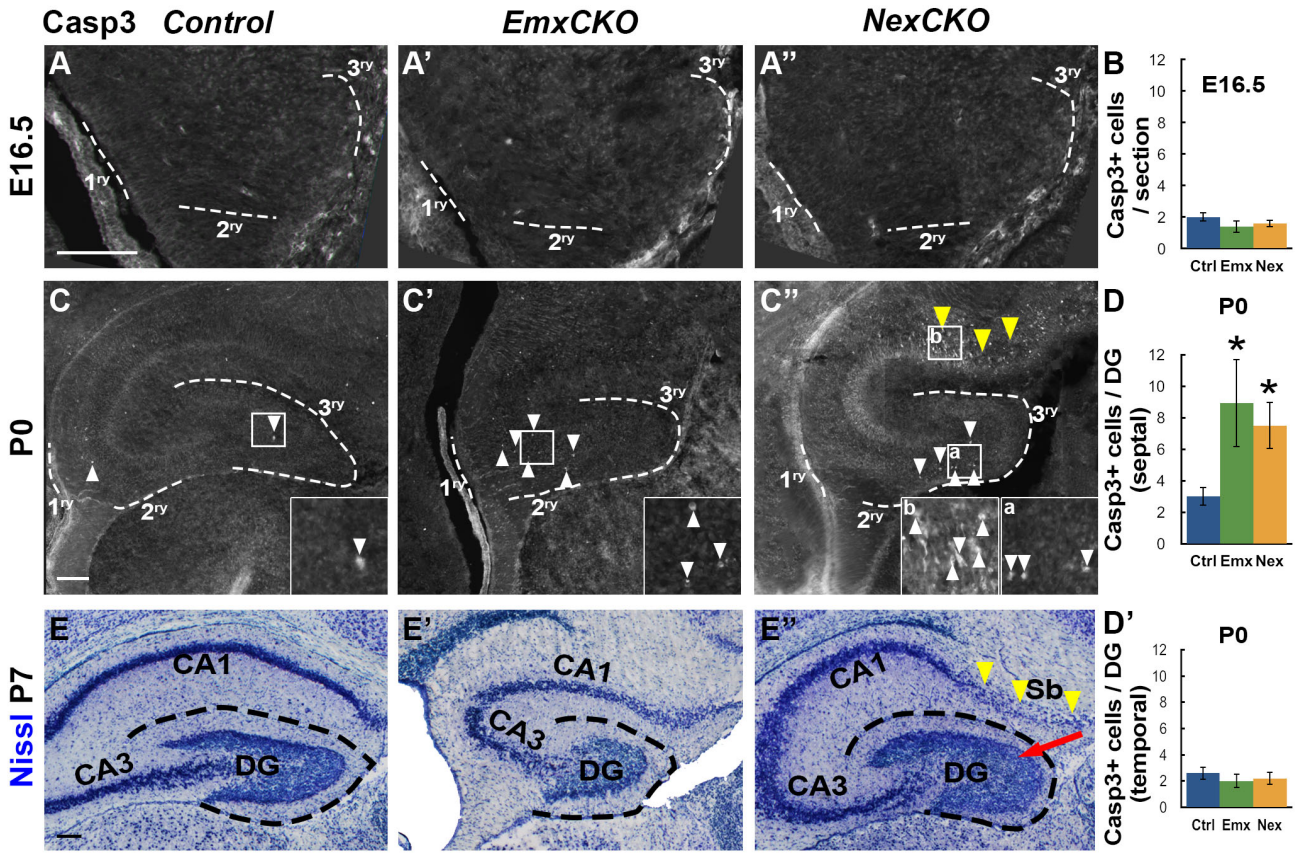

Parisot et al., Fig S5

Figure S5. Increased perinatal cell death in both *EmxCKO* and *NexCKO* dentate gyri. **(A-D)** Immunolabelling of active-Caspase3 in coronal sections of control and *COUP-TFI* mutant DGs to evaluate cell death. No increase in cell death is found at E16.5 in the 3 matrices (A-B). At P0 (C-D), significant increase of Casp3+ cells are detected in both *EmxCKO* and *NexCKO* mutant septal DG (D), whereas no differences are observed in the temporal DG (D'). Cell counts in D-D' encompass all 3 matrices of the DG at P0. White arrowheads in C-C" and their insets point to apoptotic cells in the developing DG, which are located mostly in the 2^{ry} matrix (migratory stream) in *EmxCKO* and 3^{ry} matrix in *NexCKO*. Yellow arrowheads in C" indicate an additional strong increase of Casp3+ dying cells in the subiculum (Sb) of *NexCKO*. **(E-E")** Nissl staining of P7 coronal sections of hippocampi showing cell depletion in the *NexCKO* subiculum (yellow arrowheads), which might partially explain the roundish appearance of *NexCKO* DGs (red arrow). *Scale bars: 100µm. *p≤0,05.*

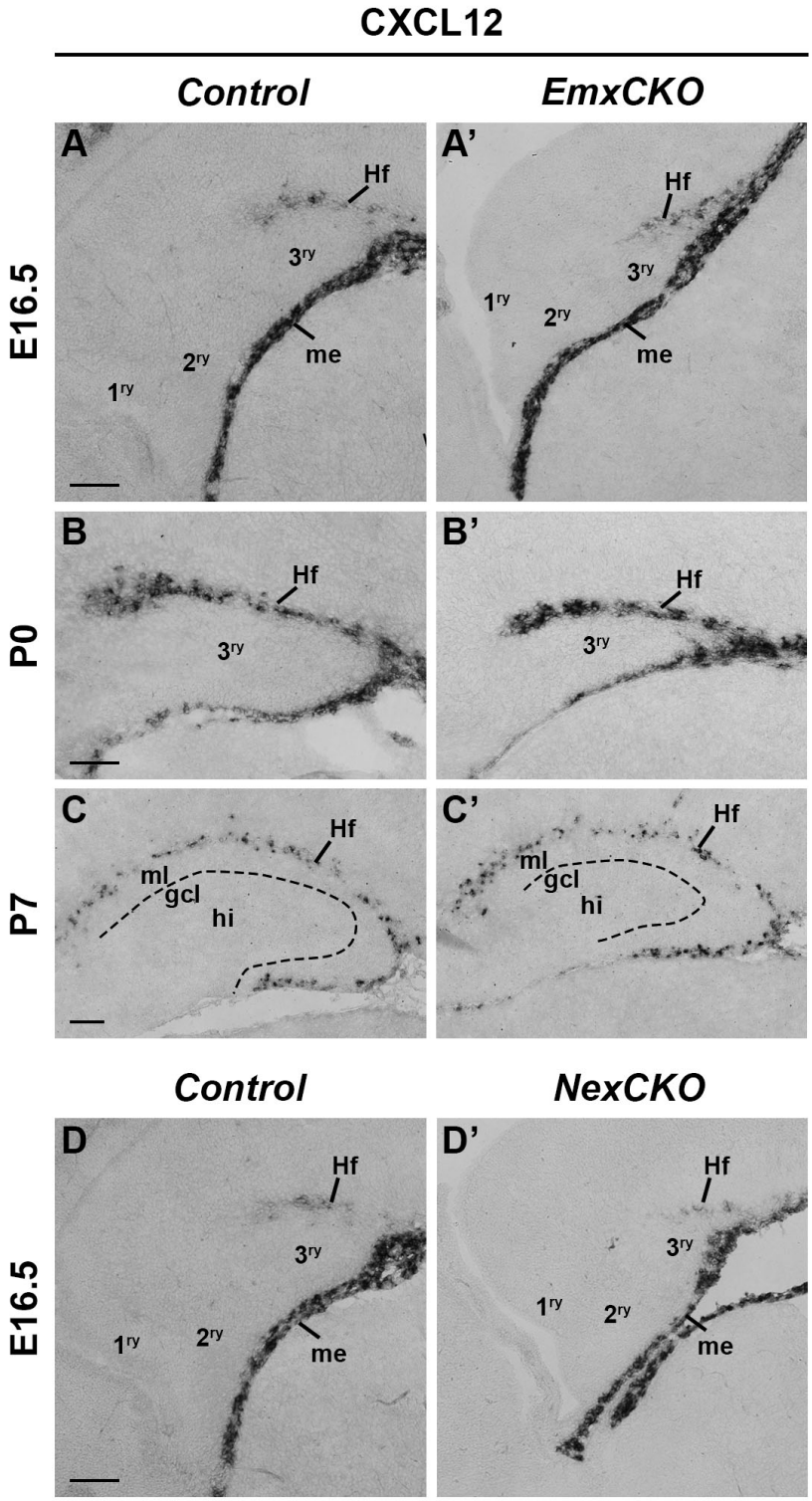

Parisot et al., Fig S6

Figure S6. Normal *CXCL12* mRNA expression in *EmxCKO* and *NexCKO* hippocampi. **(A-C')** *In situ* hybridization (ISH) of *CXCL12* transcripts in control and *EmxCKO* DGs at the indicated ages. **(D-D')** ISH of *CXCL12* in E16.5 control and *NexCKO* DGs. *gcl: GC layer; Hf: hippocampal fissure; hi: hilus; me: meninges; ml: molecular layer. Scale bars: 100µm.*

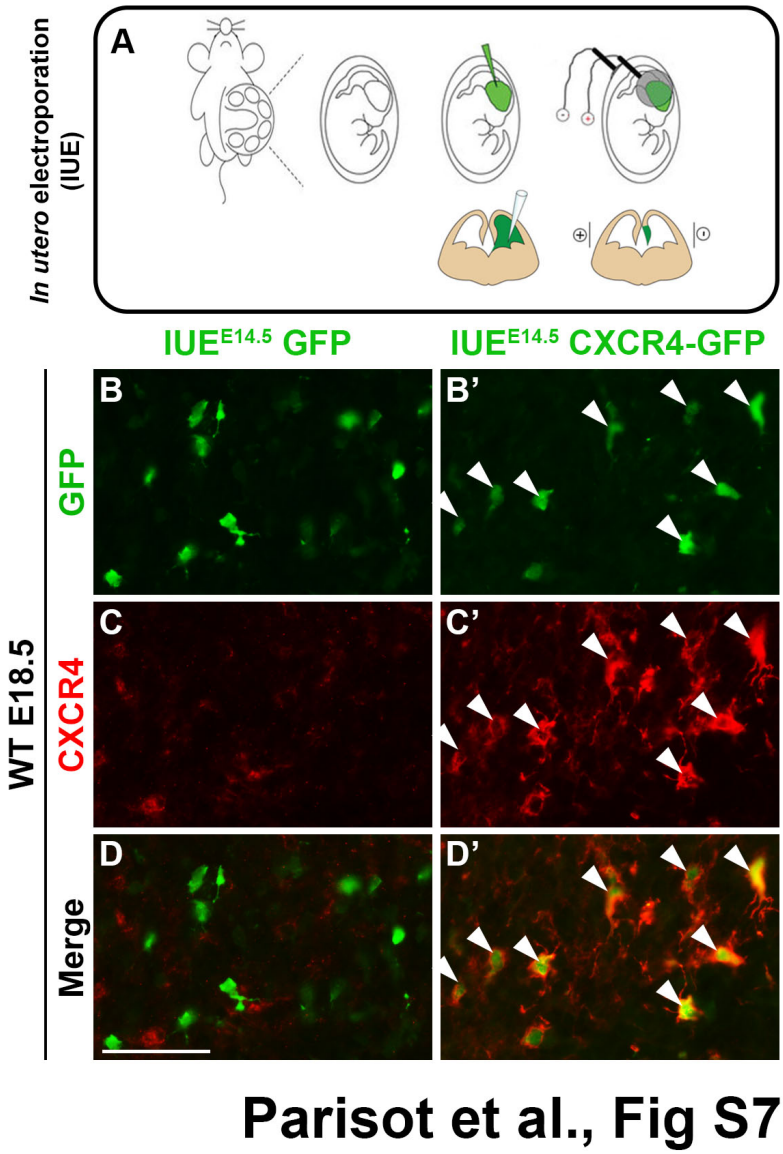

Figure S7. Electroporation of the *pCIG2-CXCR4-IRES-GFP* (CXCR4-GFP) plasmid properly express CXCR4 in GFP+ cells. (A) *In utero* electroporation strategy (images adapted from (Pacary et al., 2012)) to hit the hippocampal neuroepithelium of E14.5-old embryos. **(B-D')** Immunofluorescence for GFP and CXCR4 on E18.5 brains electroporated at E14.5 with *pCIG2-IRES-GFP* (B-D) or *pCIG2-CXCR4-IRES-GFP* (B'-D') plasmids. Pictures are taken in the CA1 region. Cells that express the CXCR4-GFP plasmid effectively overexpress CXCR4 protein (arrowheads). *Scale bar: 50µm*.

SUPPLEMENTARY MATERIALS AND METHODS

Quantitative reverse-transcriptase PCR (qRT-PCR).

Total RNA for qRT–PCR was extracted from fresh P0 hippocampi of at least 4 animals for each genotype using the NucleoSpin RNAII columns (Macherey-Nagel) following manufacturer's instructions. After RNA extraction, RNA quality was assessed with Nanodrop and gel electrophoresis. For each sample, 1mg of total RNA was reverse-transcribed using Superscript III First-Strand Synthesis System for RT–PCR (Invitrogen) following manufacturer's instructions. Amplified cDNA was quantified using KAPA SYBR FAST Master Mix (Kapa Biosystems) on a LigthCycler II 480 (Roche). Amplification take-off values were evaluated using the built-in LightCycler 480 relative quantification analysis function, and relative expression was calculated with the 2 -ΔΔCt method, normalizing with respect to the housekeeping gene ß-Actin. Fold-change variations in the levels of mRNA of interest were expressed as a percentage and normalized against WT levels (set as 100%), and standard errors were obtained from the error propagation formula. Primer sequences are listed in **Table S2**.

Quantification and statistical analysis

Volume measurements were performed using Adobe Photoshop CS6 software on the entire septo-temporal axis of Nissl-stained vibratome sections. The total, septal and temporal DG volumes of at least n=3 *EmxCKO* or *NexCKO* were calculated and compared to their respective littermate controls. The volume of the adult DG and/or hippocampus and its septo-temporal distribution was evaluated on coronal sections with the NIH *ImageJ* Software and analysed by a two-way ANOVA for repeated measures, with genotype as between group measure, and septo-temporal gradient as repeated measure. A Duncan post hoc test was used,

when appropriate, to make direct comparisons. 3D illustrations were obtained as previously described (Flore et al., 2016). Statistical significance between mutants and controls was analyzed using the Dell software *Statistica 10* and the two-tailed paired Student's t-test. Data were normalized, by defining the control value as 100%.

Cell quantification was performed on 3 coronal anatomically matched sections within the septal or temporal hippocampus of at least n=3 animals. At E16.5, 3 boxes of the same area were selected in control and mutant DG matrices. At P0, DG was delineated and separated into two areas: upper blade (UB) and lower blade (LB). At P7 and P14, DG was split into the DG three layers, based on DAPI staining. Analysis of the GFP+ cell distribution in IUE experiments was performed by counting GFP+ cells in three boxes within CA1 region and in the developing DG. Each CA1 boxes were subdivided into VZ, IZ and PCL compartments. The developing DG was subdivided into 1^{ry}, 2^{ry} and 3^{ry} matrix. The number of GFP+ cells for each compartment was expressed as a percentage of the total number of counted GFP+ cells for each region. Cell counts were performed on at least 3 consecutive rostral sections for each analysed brain using the counting tool of Adobe Photoshop CS6. A spreadsheet software and a two-tailed paired Student's t-test were used to analyse statistical significance between mutant and their controls (*p<0,05; **p<0,01; ***p<0,001). All graphs represent means ± s.e.m.

References:

Flore, G., Di Ruberto, G., Parisot, J., Sannino, S., Russo, F., Illingworth, E. A., Studer, M. and De Leonibus, E. (2016). Gradient COUP-TFI Expression Is Required for Functional Organization of the Hippocampal Septo-Temporal Longitudinal Axis. *Cereb Cortex*.

Pacary, E., Haas, M. A., Wildner, H., Azzarelli, R., Bell, D. M., Abrous, D. N. and Guillemot, F. (2012). Visualization and genetic manipulation of dendrites and spines in the mouse cerebral cortex and hippocampus using in utero electroporation. *Journal of visualized experiments : JoVE*.

Table S1. List of antibodies used in this study.

Antibody	Host species	Provider (reference)	Dilution
anti-cleaved Caspase3	rabbit	Cell Signaling (9661)	1:1000
anti-COUP-TFI	rabbit	Tripodi et al., 2004	1:1000
anti-COUP-TFI	mouse	Abcam (ab41858)	1:500
anti-GFAP	mouse	Sigma (G3893)	1:1000
anti-Ki67	rabbit	Abcam (ab833)	1:100
anti-Mcm2	rabbit	Abcam (ab4461)	1:1000
anti-NeuN	mouse	Millipore (MAB377)	1:100
anti-Prox1	rabbit	AngioBio (11-002)	1:1000
anti-Tbr1	rabbit	Abcam (ab31940)	1:1000
anti-Tbr2	chicken	Millipore (AB15894)	1:500
Alexa Fluor 488 anti-mouse/rabbit/chicken	goat	Fisher Scientific (10003482/10779623/10286672)	1:300
Alexa Fluor 555 anti-mouse/rabbit	goat	Fisher Scientific (10143952/10082602)	1:300
Alexa Fluor 647 anti-mouse/rabbit	goat	Fisher Scientific (10246452/10739574)	1:300
anti-rabbit IgG biotinylated	goat	Vector Laboratories (pk-6101)	1:300

Table S2. List of primers used in this study.

		FW	REV
for RT-PCR	COUP-TFI	TCCCATCGAAACTCTCATCC	AGTGGGCTGCTCTTGTTCC
	CXCR4	ATGGAACCGATCAGTGTGAGT	TGAAGTAGATGGTGGGCAGG
	B-Actin	ATGTGGATCAGCAAGCAGGA	GTGTAAAACGCAGCTCAGTAACA
for ChIP	CXCR4	ACAGTTCTACAGTCCTACACACAG	TCCTCTAGTTTTTGTGAGGTTTGAC